High-Dielectric Polymer Composite Materials from a Series of Mixed-Metal Phenylphosphonates, $ATi(C_6H_5PO_3)_3$ for Dielectric Energy Storage

Peter Barber, Perry J. Pellechia, Harry J. Ploehn,* and H.-C. zur Loye*

Department of Chemistry and Biochemistry and Department of Chemical Engineering, University of South Carolina, South Carolina 29208

ABSTRACT We report the preparation of new polymer composite dielectric materials for energy storage applications. New layered 1:1 mixed A^{+2}/Ti^{4+} metal phenylphosphonates, $ATi(O_3PC_6H_5)_3$, A = Mg, Ca, Sr, Ba, and Pb, have been prepared via a melt route, in which mixed metal oxides, $ATiO_3$, were reacted with molten phenyl phosphonic acid. The mixed-metal phosphonates were combined with polystyrene (PS) via a solution route and cast as thin films for dielectric permittivity measurements. The $ATi(O_3PC_6H_5)_3$−PS composites exhibit a substantial enhancement in the dielectric permittivity as a function of weight loading relative to the parent $ATiO_3$−PS composites. For both $ATiO_3$−PS and $ATi(O_3PC_6H_5)_3$−PS, the composites' dielectric permittivity increases with A cation polarizability. Unusually large increases for 40 wt % $ATi(O_3PC_6H_5)_3$−PS composites (A = Sr, Ba, and Pb) indicate permittivity enhancement that goes beyond the effect of varying filler composition.

KEYWORDS: polymer composite • mixed-metal phosphonate • dielectric permittivity • solid-state ^{31}P NMR • polymer composite film • polystyrene

INTRODUCTION

Electrical energy storage plays a key role in mobile electronic devices, stationary power systems, hybrid electrical vehicles, and pulse power applications (1, 2). In particular, there exists a growing need for capacitors that can accumulate a large amount of energy and then deliver it nearly instantaneously. This kind of "pulse power" is needed for a variety of military and commercial applications. Over time, these applications demand ever-higher energy and power densities as well as higher rate capability. Existing dielectric capacitors have low energy densities, both on a volume and on a mass basis. The volumetric density $\breve{W}$ (J/cm^3) stored by a dielectric capacitor is given by

$$\breve{W} = \int E dD$$

where E is the applied electric field and D is the electric displacement. For the idealized case of a linear dielectric satisfying $D = \varepsilon_0\varepsilon_r E$ (dielectric constant ε_r), subjected to a field as large as the breakdown field strength E_{bd}, the theoretical maximum volumetric energy density is

$$\breve{W} = \frac{1}{2}\varepsilon_0\varepsilon_r E_{bd}^2$$

The most obvious way to increase $\breve{W}$ is to choose dielectric materials with the highest possible values of ε_r and E_{bd}. Thermoplastic polymers such as polypropylene or polystyrene exhibit a high breakdown field strength (≥600 V/μm), but have very low dielectric constants ($\varepsilon_r \leq 3$) (1). The dielectric constant for ferroelectric ceramics, such as $BaTiO_3$, can be in excess of 1000; however, due to defect-rich networks in ceramics, the breakdown field strengths are generally low and thus limit their use for high energy density power storage (3). For nonlinear materials that manifest dielectric saturation under high applied fields, it is clear that maximizing ε_r does not necessarily maximize $\breve{W}$ (13).

Polymer−ceramic composites, consisting of both high dielectric ceramics and high breakdown voltage polymers, offer tremendous potential for combining the advantages of both components for producing capacitors suitable for pulse power technologies. Not surprisingly, the dielectric properties of polymer−ceramic composites are being actively investigated (4, 5). Recent work to incorporate high dielectric nanofillers, such as $BaTiO_3$ (6−9) and TiO_2 (10−12), into polymer matrices has resulted in moderate improvements in the dielectric permittivity but typically require high inorganic weight loadings (≥40 vol %). A significant problem that arises from high inorganic weight loadings in polymers is poor dispersion of the filler in the polymer matrix. This may result in effective dielectric permittivity values lower than one might expect on the basis of various theoretical models of composite dielectrics. However, a more serious

* To whom correspondence should be addressed TEL: (803) 777-6916 (H.-C.z.L.); (803) 777-7307 (H.P.). FAX: (803) 777-8508 (H.-C.z.L.); (803) 777-8265 (H.P.). E-mail: zurloye@mail.chem.sc.edu (H.-C.z.L.); ploehn@engr.sc.edu, (H.P.).
Received for review May 6, 2010 and accepted August 17, 2010

DOI: 10.1021/am1003987

consequence is the reduction of E_{bd} relative to that of the pure polymer resulting from the aforementioned defect-rich inorganic filler network. Conventional blending of the inorganic additive and the polymer host matrix often leads to inhomogeneities and aggregation of the inorganic phase.

This problem can sometimes be averted by surface modifying the inorganic filler with organic moieties that are chemically similar to the polymer host matrix of the composite. Recently Kim et al. showed that for $BaTiO_3$, phosphonic acids effectively modify the surface of $BaTiO_3$ (9, 13). Our research group also successfully utilized phosphonic acids to modify $BaTiO_3$. In addition to simple surface modification, we changed the reaction conditions to utilize the mineralizing and chelating properties of phosphonic acids to synthesize a new class of layered mixed-metal phosphonates (14). In both cases, the composites made using the organically modified inorganic fillers drastically improved the overall dielectric performance of the composite relative to the unmodified ceramic.

The most common structural motif for metal phosphonates is that of a lamellar structure type (14, 15). In these solids, the phosphonate oxygens bond strongly to the metal ions, forming a tightly bound inorganic lamellae. These inorganic layers can be built from planes of metal atoms with phosphonate groups lying above and below the plane. The phosphonates are bonded to two or three different metal atoms, and this arrangement forces the phosphorus–carbon bond to protrude into the interlayer region of the lamellae. This protrusion of the organic group into the interlayer space creates an organic bilayer system between the inorganic lamellae.

Many diverse organic groups can be incorporated into phosphonic acid derivatives, reacted with transition metal, and crystallized into a layered metal phosphonate structure. Because of this organic flexibility, metal organo-phosphonates have found a wide variety of applications, ranging from ion exchange materials (16), porous materials (17), catalysts (18, 19), dielectric coatings (20, 21), magnetism (22–28), and recently, luminescence (29).

As mentioned in our previous work, complexing agents such as oxalic acid have been used to sequentially dissolve mixed metal oxides. Specifically, Figueroa et al. illustrated the solubilities of simple metal oxides under aqueous conditions (32), where oxalic acid was used as a chelating agent that enabled the formation of soluble mixed metal oxalate species. Using this approach with phenylphosphonic acid as the complexing agent, we were able to synthesize mixed-metal phosphonates. However it has also been shown by the works of Carlino et al. and Hix et al. that mixed metal phosphonates can also be obtained from the reaction between mixed metal oxides and molten phosphonic acids (33, 34).

In this paper, we present the synthesis of new mixed-metal phenylphosphonates with the formula $ATi(C_6H_5PO_3)_3$, where A = Mg, Ca, Sr, Ba, and Pb, from the reaction between molten phenylphosphonic acid and $ATiO_3$ (A = Mg, Ca, Sr, Ba, and Pb) perovskites. Results from ^{31}P-MAS NMR experiments demonstrate that the metal centers are intimately mixed, so these materials are not simply mixtures of single metal phosphonates. This builds upon our previous report (wherein A = Sr, and Ba) to show the generality of the synthesis method for a sequence of five +2 valent A cations.

Unfortunately, thermal decomposition at around 500 °C makes it impossible to sinter these mixed metal phosphonates into pellets suitable for direct characterization of dielectric properties. Primarily for this reason, we prepared composites of these materials dispersed in polystyrene (PS) in order to compare their dielectric properties within the phosphonate group and with the parent oxides. The paper concludes with a discussion of the trends in the dielectric permittivities of these composites as a function of the A cation.

2. EXPERIMENTAL SECTION

2.1. Starting Materials. Barium titanate (99+%, nanopowder), strontium titanate (99+%, nanopowder), and calcium titanate (99+%, nanopowder) were purchased from Aldrich and used without further purification. Magnesium titanate (99%) and lead titanate (99.5%) were purchased from Alfa Aesar, and sonicated for 1.5 h in ethanol before use to reduce particle agglomeration. Phenyl phosphonic acid (98%) was purchased from Acros Organics and used as received. Polystyrene (PS, $M_w \approx 192\,000$) was purchased from Aldrich and used as received.

2.2. Preparation of $ATi(C_6H_5PO_3)_3$ (A^{2+} = Mg, Ca, Sr, Ba, and Pb). Each titanate was intimately mixed with stoichiometric amounts of the phenyl phosphonic acid for 30 min using a mortar and pestle. The resulting mixture was placed into a thick Pyrex tube, which was sealed with a Teflon screw cap. The powder was heated to slightly above the melting point of phenyl phosphonic acid (168 °C) for 24 h. All reactions produced a white powder, which was washed with 95% ethanol/water to remove unreacted materials, and centrifuged to isolate the pure product. The final products were dried overnight at 80 °C in a convection oven. For simplicity, the compositions $ATi(C_6H_5PO_3)_3$ will be written as $MgTi(PPA)_3$, $CaTi(PPA)_3$, $SrTi(PPA)_3$, $BaTi(PPA)_3$, and $PbTi(PPA)_3$.

2.3. Preparation of $ATi(PPA)_3$–PS and $ATiO_3$–PS Composite Films. Appropriate amounts of inorganic materials ($ATiO_3$ and $ATi(PPA)_3$) were dispersed in toluene and ball-milled for 12 h. The resulting solution was heated to 70 °C under constant stirring. Polystyrene (PS) was added to the heated solution and allowed to dissolve. The viscosity of the solution was controlled through the evaporation/addition of toluene. The PS–inorganic slurry was spin-coated for 15 s at 1000 rpm onto a silicon wafer. The spin-coated films were air-dried before being peeled off the silicon wafer. The average thicknesses of the PS composite films were ~25 μm as measured via micrometer. Finally, parallel plate capacitors were formed by sputter-depositing gold as the top and bottom electrodes onto the film surface through a shadow mask.

2.3. Characterization. FT-IR spectra were recorded on a Perkin-Elmer Spectrum 100 using an ATR diamond cell attachment.

Powder X-ray diffraction patterns were collected using a Rigaku DMAX 2200 diffractometer using Cu Kα radiation.

Thermogravimetric analyses were performed using a Thermal Analysis (TA) SDT-Q600 simultaneous DTA/TGA system in an oxidizing environment. Samples were heated in air to 800 °C using a heating rate of 10 °C/min.

Solid-state ^{31}P NMR spectra were collected on a Varian Inova 500 spectrometer operating at 202.489 MHz using a Doty Scientific 4 mm/XC magic angle spinning (MAS) probe. Bloch decays of 50 ms were collected with a 200 ppm window after 45 degree excitation pulses. A relaxation delay of 10 s was used

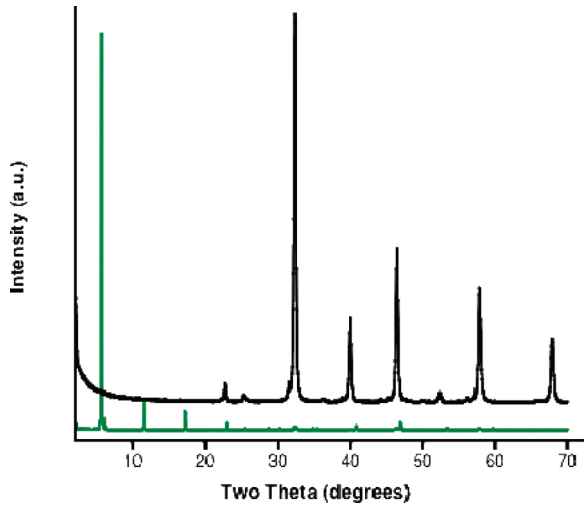

FIGURE 1. Powder X-ray diffraction patterns of $SrTi(PPA)_3$ in green and $SrTiO_3$ in black.

Table 1. Listing of the Interlayer Spacing for the Mixed-Metal Phenylphosphonate Compounds

compd	interlayer spacing (Å)
$MgTi(PPA)_3$	14.3(1)
$CaTi(PPA)_3$	15.6(1)
$SrTi(PPA)_3$	15.5(1)
$BaTi(PPA)_3$	15.7(1)
$PbTi(PPA)_3$	15.5(1)

between each transient. TPPM dipolar decoupling with a field strength of 45 kHz was applied during acquisition. A MAS speed of 10 kHz was used, and between 16 and 64 scans were collected for each run. Spectral deconvolution was performed with the standard routine included with Varian's VNMR 6.1C software.

A Solartron SI 1287 Electrochemical Interface coupled with Schlumberger SI 1260 Impedance/Gain-Phase Analyzer was used to measure the capacitance using ZPlot and ZView software. The dielectric constants were calculated from the capacitance values and the measured film thicknesses and areas.

3. RESULTS

3.1. Powder X-ray Diffraction. The phase purity of the final products was checked by powder X-ray diffraction. Figures 1 and S1 (see the Supporting Information) show the diffraction patterns of the starting oxides ($ATiO_3$) and the corresponding phenylphosphonate products [$ATi(PPA)_3$]. The diffraction patterns for all the mixed-metal phenylphosphonates consist of several evenly spaced low-angle peaks that are characteristic of 00 L reflections of layered solids, which is consistent with our previous report on $BaTi(PPA)_3$ and $SrTi(PPA)_3$ (14). Only slight variations in the interlayer spacing are observed in the diffraction patterns, listed in Table 1. Because all of the mixed-metal phosphonates contain the same phenyl pendant group, the small variation in interlayer separation is caused primarily by the change in the size of the A cation.

3.2. ^{31}P-MAS NMR Experiments. ^{31}P-MAS NMR experiments were carried out on all of the mixed-metal phenylphosphonates to investigate the phosphorus environments. As discussed in our previous report on $BaTi(PPA)_3$ and $SrTi(PPA)_3$ (30), powder X-ray diffraction does not provide sufficient enough evidence of a true mixed-metal phosphonate versus a physical mixture of the individual metal phosphonates. The phosphorus environments in a single divalent metal phosphonate are quite different from a single tetravalent phosphonate. This difference arises from the crystal structure differences between divalent and tetravalent phosphonate systems. In a divalent phosphonate, for example Ba(PPA) (31), the coordination environment around each Ba^{2+} cation consists of six oxygens, two belonging to a single phosphonate group, three belonging to three different phosphonate groups, and one that is part of a water molecule; each phosphonate group bridges three Ba^{2+} cations. A consequence of this structural arrangement is that each BaO_6 octahedron is connected via a shared oxygen to four other BaO_6 octahedra. By comparison, in a tetravalent metal phosphonate, such as $Ti(PPA)_2$, the octahedral coordination sphere around each Ti^{4+} cation consists of six oxygens from six different phosphonate groups. Each phosphonate group bridges three different Ti^{4+} cations. A consequence of this structural arrangement is that the TiO_6 octahedra are isolated from each other. In both phosphonate cases, the crystal structure suggests that there should only be one unique phosphorus environment. This has been confirmed by numerous ^{31}P NMR studies on divalent and tetravalent phosphonates (30).

The ^{31}P MAS NMR spectra (Figure 2) for the mixed metal phosphonates all show three distinct phosphorus shifts, not one. The first phosphorus peak for the $MgTi(PPA)_3$ compound at −3.95 ppm (s) is assigned to the Ti−O−P environment, the second phosphorus environment at 12.43 ppm (s) is assigned to the Mg−O−P environment, and the third phosphorus environment at 3.40 ppm (s) in the $MgTi(PPA)_3$ NMR spectra is assigned to contributions from both the M^{2+}−O-P and the M^{4+}−O−P environment; this latter phosphorus environment is of the bridging type M^{2+}−O−P−O−M^{4+}. In $CaTi(PPA)_3$ we observe the shift assigned to Ti−O−P at −4.05 ppm (s), the bridging phosphorus at 3.31 ppm (s), and the Ca−O−P shift at 12.31 ppm (s). In $SrTi(PPA)_3$, we observe the shift assigned to Ti−O−P at −4.31 ppm (s), the bridging phosphorus at 3.15 ppm (s), and the Sr−O−P shift at 10.08 ppm (s). In $BaTi(PPA)_3$ we observe the shift assigned to Ti−O−P at −3.92 ppm (s), the bridging phosphorus at 3.38 ppm (s), and the Ba−O−P shift at 9.25 ppm (s). In $PbTi(PPA)_3$, we observe the shift assigned to Ti−O−P at −3.98 ppm (s), the bridging phosphorus at 3.28 ppm (s), and the Ca−O−P shift at 12.45 ppm (s). These NMR spectra show conclusively that the metal centers are intimately mixed and bridged by phosphonate groups, rather than existing as physical mixtures of the single metal phosphonates (30).

3.3. Thermal Analysis. Thermogravimetric analysis experiments were used to determine the thermal stability of the mixed-metal phosphonates and to help determine the chemical formula for the mixed-metal phenylphosphonates. All of the mixed-metal phenylphosphonates show thermal stabilities greater than or equal to 500 °C. The observed

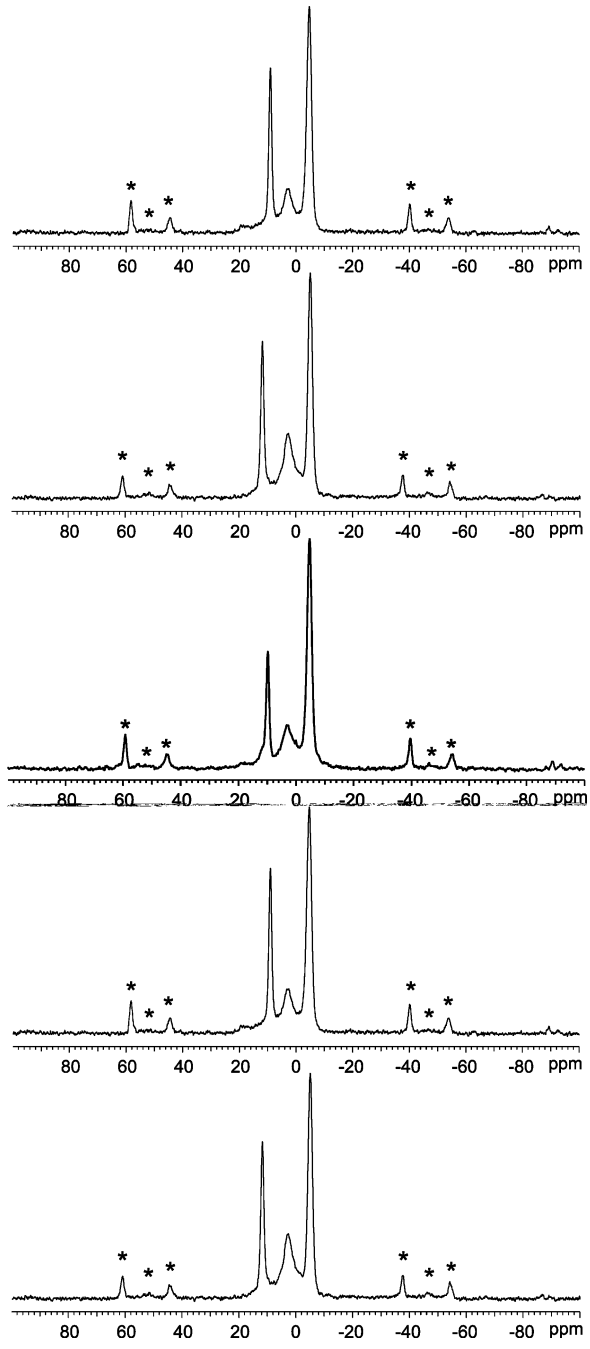

FIGURE 2. ^{31}P-MAS NMR spectra of the mixed-metal phosphonates. From top to bottom, $MgTi(C_6H_5PO_3)_3$, $CaTi(C_6H_5PO_3)_3$, $SrTi(C_6H_5PO_3)_3$, $BaTi(C_6H_5PO_3)_3$, $PbTi(C_6H_5PO_3)_3$. The peaks marked by * are spinning side bands.

weight losses for the mixed-metal phenylphosphonates are in good agreement with the weight losses expected for the loss of the phenyl group and are summarized along with the thermal stabilities of each of the mixed-metal phenylphosphonates in Table 2.

3.4. Dielectric Properties of Polystyrene Composites. Figure 3 shows the relative permittivities (dielectric constants) as functions of inorganic weight loading for polystyrene (PS) composites incorporating the unmodified titanates ($ATiO_3$) and the corresponding mixed-metal phenylphosphonates ($ATi(PPA)_3$); numerical values are summarized in Table 3. For the $ATiO_3$—PS composites at 10 wt % inorganic filler loading, all of the relative permittivity values were close to that of pure PS (2.6 ± 0.1). In particular, the values for 10 wt % $MgTiO_3$—PS and $CaTiO_3$—PS are about 20% less and 14% more than that of pure PS, respectively. This suggests that the intrinsic relative permittivities of these titanates do not differ much from that of PS. For the Sr, Ba, and Pb titanates at 10 wt % in PS, the permittivity values are no more than twice that of pure PS. Upon a 4-fold increase in $ATiO_3$ weight loading to 40 wt %, the composite permittivity values approximately double relative to the values at 10 wt %.

Table 2. Theoretical versus Observed Weight Loss and Decomposition Temperature for the Mixed-Metal Phenylphosphonates

mixed-metal phosphonate	theoretical weight loss percent	observed weight loss percent	degradation temperature (°C)
$MgTi(PPA)_3$	38.4	37.2	500
$CaTi(PPA)_3$	37.3	36.8	515
$SrTi(PPA)_3$	34.3	34.3	510
$BaTi(PPA)_3$	31.7	31.1	500
$PbTi(PPA)_3$	28.7	29.6	525

Considering the $ATi(PPA)_3$—PS composites, the relative permittivity of every sample (for each A cation and at both weight loadings) was substantially greater than that of the corresponding $ATiO_3$—PS composite. For example, the permittivity of the 10 wt % $MgTi(PPA)_3$—PS composite is 78% greater than that of pure PS, and 125% greater than that of the corresponding 10 wt % $MgTiO_3$—PS composite made with the parent titanate. Substantial increases are also observed for 40 wt % $MgTi(PPA)_3$—PS, and $CaTi(PPA)_3$—PS (both loadings) relative to the corresponding $ATiO_3$—PS composites. For $SrTi(PPA)_3$—PS, $BaTi(PPA)_3$—PS, and $PbTi(PPA)_3$—PS composites, the permittivity values are between 57% and 124% greater than those of the corresponding $ATiO_3$—PS composites. These results suggest that, regardless of the A cation, the presence of the phenylphosphonate groups in the materials and phenyl groups in the interlayer space leads to a significant increase in the permittivity of the $ATi(PPA)_3$—PS composites compared to the $ATiO_3$—PS composites. Indirectly, this suggests that the permittivities of the neat mixed-metal phenyl phosphonates are probably substantially greater than those of the corresponding parent mixed-metal titanates. Of course, differences in quality of inorganic particle dispersion in the PS and other interfacial phenomena may also play a role.

It is interesting to note that single-metal phenylphosphonates have low dielectric constants and are in fact being investigated as low dielectric constant materials to replace silicon dioxide as an interlayer dielectric in future microelectronic devices (30, 35—38). The presence of two metals within the phenylphosphonate structure certainly seems to enhance the relative permittivity.

Figure 3 (right panel) also shows that the relative permittivities of $SrTi(PPA)_3$—PS, $BaTi(PPA)_3$—PS, and $PbTi(PPA)_3$—PS composites increase with filler weight loading at a higher rate than the corresponding $ATiO_3$—PS composites. Upon a 4-fold increase in $ATi(PPA)_3$ weight loading (from 10 to 40

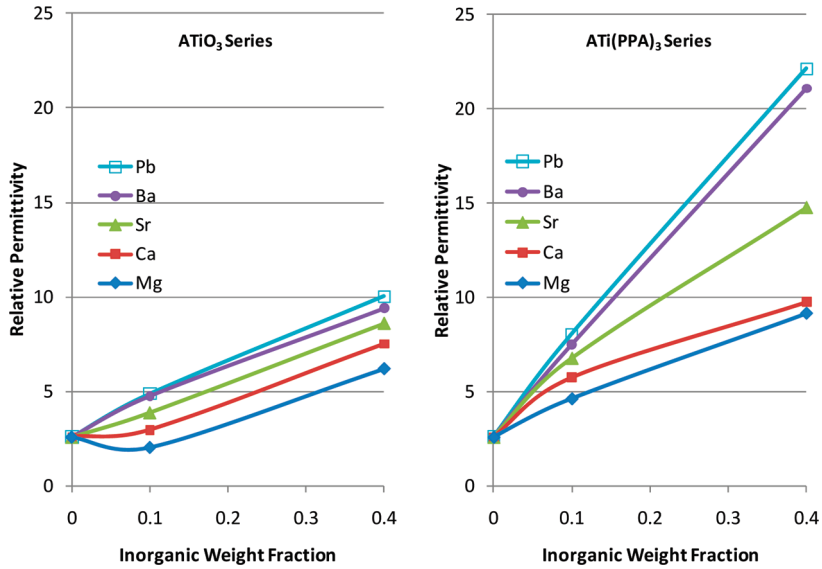

FIGURE 3. Relative dielectric permittivity of $ATiO_3$–PS and $ATi(PPA)_3$–PS composites as functions of inorganic filler loading (weight fraction) and A cation.

Table 3. Comparison of the A-cation Polarizability and the Respective Dielectric Constants of the Titanate and Phenylphosphonate–PS Composites

A^{2+} cation	polarizability[a] α (Å^3)	ε_r 10 wt % $ATiO_3$–PS	ε_r 10 wt % $ATi(PPA)_3$–PS	ε_r 40 wt % $ATiO_3$–PS	ε_r 40 wt % $ATi(PPA)_3$–PS
Mg	0.58	2.06 ± 0.2	4.64 ± 0.2	6.21 ± 0.2	9.16 ± 0.2
Ca	1.22	2.95 ± 0.2	5.75 ± 0.2	7.52 ± 0.2	9.75 ± 0.2
Sr	1.79	3.89 ± 0.2	6.78 ± 0.2	8.60 ± 0.2	14.76 ± 0.2
Ba	2.44	4.77 ± 0.2	7.49 ± 0.2	9.40 ± 0.2	21.09 ± 0.2
Pb	3.68	4.88 ± 0.2	8.05 ± 0.2	10.02 ± 0.2	22.12 ± 0.2

[a] See ref 39.

wt %), the composite permittivity values increase by 118%, 182%, and 175% for A = Sr, Ba, and Pb, respectively. For A = Mg and Ca, the same increase in weight loading merely doubles the composite permittivity, as found for all of the titanate composites. We do not have a definitive explanation for this observation at this point. However, we speculate that the steeper increase with filler loading observed for $SrTi(PPA)_3$–PS, $BaTi(PPA)_3$–PS, and $PbTi(PPA)_3$–PS composites may be due to smaller particle size, different polycrystalline structure, and/or better dispersion of the inorganic filler in the PS. Further experiments will be needed to investigate this question.

Finally, Figure 3 shows that for both the $ATiO_3$ and $ATi(PPA)_3$ series of composites, the relative permittivity increases in the order Mg < Ca < Sr < Ba < Pb, which corresponds to increasing A cation polarizabilities (Table 3). This trend may not be surprising because one might expect that the relative permittivity of a material should increase with the polarizabilities of the constituent atoms. Hence the permittivity trend with varying A cation implies that the intrinsic relative permittivity of the pure $ATi(PPA)_3$ materials also increases in the same order.

However, there may be other factors that play a role besides the identity of the A cation. Figure 4 shows the relative permittivities of $ATiO_3$–PS and $ATi(PPA)_3$–PS composites plotted versus the A cation polarizability. Although permittivity increases monotonically with A cation polarizability, the increase is not linear, suggesting that other factors

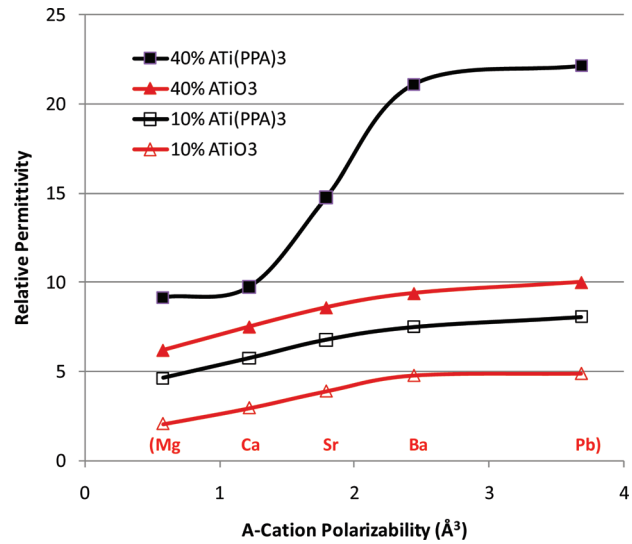

FIGURE 4. Relative dielectric permittivity of $ATiO_3$–PS and $ATi(PPA)_3$–PS composites as functions of A cation polarizability (A cation identities indicated above ordinate axis).

must be significant. In particular, in all cases, the permittivity increase appears to level off going from A = Ba to Pb. Incremental changes in the unit-cell structure and dimensions with varying A cation influence the permittivity of the crystal and may be partially responsible. This question cannot be addressed until we are able to obtain single-crystal structures of these materials.

Figure 4 also shows that the trend for the 40 wt % $ATi(PPA)_3$−PS composites clearly differs from the others. Although a definitive explanation requires further experimental work, we speculate that the phenylphosphonate group may result in better dispersion and electromagnetic isolation of polarizable domains. This may enable the filler phase (comprising both the inorganic layers and phenyl phosphonate interlayers) to carry a higher density of electromagnetic field lines as the filler loading increases. The effect should be more pronounced for the Sr, Ba, and Pb A cations if the permittivities of these phenylphosphonates are significantly higher than those based on Mg and Ca.

4. DISCUSSION

The reaction between alkali-metal titanium perovskites ($ATiO_3$) and molten phenylphosphonic acids is related to the well-known dissolution reactions between mixed metal oxides and chelating species, such as oxalic acid, which result in the formation of metal complexes. It has been determined that after an initial incongruent dissolution of a small fraction of the solid, the dissolution becomes congruent and both metals are transferred at the same rate during the dissolution reaction (32). When a phosphonic acid is used as the chelating agent, the resulting product is not a molecular metal complex, but rather a mixed-metal extended structure. As we showed in our previous report, the phosphonate formed during this dissolution process contains both cations from the precursor perovskites in a 1:1 ratio, which was confirmed by several techniques such as XPS (bulk) and HRTEM/EDS (platelet) (30) .

The structure of the alkali-metal titanium phenylphosphonates and purity were investigated by powder X-ray diffraction. The XRD data, shown in Figure 1 and Figure S1a−S1d in the Supporting Information, are consistent with lamellar structures, similar to what is found in simple metal phosphonates. The corresponding interlayer separations, listed in Table 1, are consistent with a mixed-metal layer held together on both sides by phenyl phosphonic acids whose phenyl groups extend into the interlayer space. The ^{31}P NMR data indicate the presence of three distinct phosphorus environments, as would be expected for this type of mixed-metal structure. One phosphorus environment is generated by the M^{2+}−O−P linkage, a second by the Ti^{4+}−O−P linkage, and a third by the M^{2+}−O−P−O−Ti^{4+} bridging phosphorus linkage.

The ability to prepare a series of isostructural layered mixed metal phosphonates enables us to investigate the impact of the identity of the A cation on the dielectric properties of polystyrene composites made from these materials. One would expect that the permittivity of the mixed metal phosphonates would increase for the more polarizable A cations, resulting in an enhanced dielectric constant for the composite. All the mixed metal phosphonates were readily dispersed in toluene, which is necessary in order to obtain films with uniform filler dispersion. Films were readily obtained by spin coating these solutions. Typical films were $\sim 25\,\mu$m thick and were clear and transparent, an indication of good filler dispersion. Free-standing films are easily obtained by removing the film from the spin coating substrate. All composite films were compared to freestanding polystyrene films, which have a measured dielectric constant of 2.6, consistent with a reported dielectric constant of ∼2−3, as well as to composite films consisting of the perovskite oxide precursor dispersed in PS.

There are many models that try to relate the permittivity of the composite to the permittivity of the constituent components (4). Although the dielectric constant of PS is readily measured, the inability to prepare dense pellets of the mixed-metal phenylphosphonates due to sample decomposition at the temperatures needed to achieve sintering, has precluded us from determining the intrinsic dielectric permittivities of these phosphonates. Thus we were unable to use these models to predict the permittivity of our composites and to see how well the models match our data.

The addition of the mixed metal (A−Ti) phenylphosphonates greatly increased the relative permittivity of the composite up to a maximum value of ∼22 for 40 wt % loading of BaTi(PPA) and PbTi(PPA) in polystyrene (Figure 3 and Table 3). Moreover, the A−Ti phenylphosphonate composites all exhibited significantly greater permittivities than those based on the parent $ATiO_3$ materials. For both the $ATiO_3$−PS and $ATi(PPA)_3$−PS composites, the composites' relative permittivity increases monotonically with the A cation polarizability. Taken together, these observations imply that the dielectric properties of these composites are dominated by the intrinsic permittivities of the $ATiO_3$ and $ATi(PPA)_3$ filler materials, as expected. Moreover, trends in the fillers' intrinsic permittivity can be inferred from measurements of the relative permittivity of their polystyrene composites. Nonetheless, a possible synergistic effect of the phenylphosphonate group in promoting better dispersion and electromagnetic energy storage by the filler can be seen in the dependence of permittivity on filler loading (Figure 3) and on A cation polarizability (Figure 4).

5. CONCLUSIONS

We have successfully synthesized new members of the mixed-metal phenylphosphonate family, $ATi(PPA)_3$, where A = Mg, Ca, Sr, Ba, and Pb. In all cases, PS composites containing $ATi(PPA)_3$ have significantly greater dielectric permittivities than composites containing that parent $ATiO_3$ material. Incorporation of A site cations with greater polarizability also increases ther permittivity of composites containing these fillers. Our results indicate that one can measure the dielectric properties of a closely related set of composites to infer trends in the properties of the filler materials. The observations in this work are consistent with the expectation that the incorporation of elements and organic groups with greater polarizability increases the dielectric permittivity of the mixed metal phosphonates.

Acknowledgment. Financial support for this research was provided by the United States Air Force Award FA9550-08-10377.

Supporting Information Available: X-ray diffraction patterns of the starting oxides ($ATiO_3$) and the corresponding

phenylphosphonate products [ATi(PPA)$_3$] for A= Mg, Ca, Ba, and Pb, as well as *d* spacing information for all materials (PDF). This material is available free of charge via the Internet at http://pubs.acs.org.

REFERENCES AND NOTES

(1) Nalwa, H. *Handbook of Low and High Dielectric Constant Materials and their Applications*; Academic Press: London, 1999.
(2) Osaka, T.; Datta, M. *Energy Storage Systems for Electronics; Gordon and Breach*: Amsterdam, The Netherlands, 2001.
(3) Arlt, G.; Hennings, D.; de Witt, G. *J. Appl. Phys.* **1985**, *58*, 1619.
(4) Barber, P.; Balasubramanian, S.; Anguchamy, Y. K.; Gong, S.; Wibowo, A.; Gao, H.; Ploehn, H. J.; zur Loye, H.-C. *Materials* **2009**, *2*, 1697–1733.
(5) Lu, J.; Wong, C. P. *IEEE Trans. Dielect. Elect. Insul.* **2008**, *15*, 1322.
(6) Badheka, P.; Magadala, V.; Devaradju, N. G.; Lee, B. I.; Kim, E. S. *J. Appl. Polym. Sci.* **2005**, *99*, 2815.
(7) Badheka, P. M. V.; Devaraju, N. G.; Lee, B. I.; Kim, E. S. *J. Appl. Polym. Sci.* **2006**, *99*, 2815.
(8) Devaraju, N. G.; Kim, E. S.; Lee, B. I. *Microelectron. Eng.* **2005**, *82*, 71–83.
(9) Kim, P. J.; Simon, C.; Hotchkiss, Peter, J.; Haddock, Joshua, N.; Kippelen, Bernard; Marder, Seth, R.; Perry, Joseph, W. *Adv. Mater.* **2007**, *19*, 1001–1005.
(10) Dang, Z. M. *Adv. Mater.* **2003**, *15*, 1625–1629.
(11) Deskins, N. A.; Dupuis, M. *Phys. Rev. B* **2007**, *75*, 1952121–10.
(12) Li, J. J.; Seok, S. I.; Chu, B. J.; Dogan, F.; Zhang, Q. M.; Wang, Q. *Adv. Mater.* **2009**, *21*, 217–221.
(13) Kim, P.; Doss, N. M.; Tillotson, J. P.; Hotchkiss, P. J.; Pan, M.-J.; Marder, S. R.; Li, J.; Calame, J. P.; Perry, J. W. *ACS Nano* **2009**, *3*, 2581–2592.
(14) Clearfield, A. *Curr. Opin. Solid State Mater. Sci.* **1996**, *1*, 268–278.
(15) Clearfield, A. *Curr. Opin. Solid State Mater. Sci.* **2002**, *6*, 495–506.
(16) Alberti, G. C.; Constantino, U.; Vivani, R. *Adv. Mater.* **1996**, *8*, 291.
(17) Clearfield, A. *Dalton Trans.* **2008**, 6089.
(18) Curini, M. R.; Constantino, U. *Curr. Opin. Org. Chem.* **2004**, *8*, 591.
(19) Zhang, X.-J.; Yuan, Z.-Y. *J. Mater. Chem.* **2008**, *18*, 2003.
(20) Katz, H. E. *Chem. Mater.* **1993**, *5*, 1162.
(21) Schilling, M. L.; Stein, S. M.; Shane, S.; Wilson, W. L.; Ungashe, S. B.; Taylor, G. N.; Putvinski, T. M.; Chidsey, C. E. *Langmuir* **1993**, *9*, 2156.
(22) Bujoli, B. P.; Palvadeau, P.; Le Bideau, J.; Payen, C.; Rouxel, J. *Chem. Mater.* **1993**, *5*, 583.
(23) Rabu, P. J.; Bujoli, B. P. *J. Mater. Chem.* **1999**, *9*, 1323.
(24) Bellitto, C. B.; Righini, E. M. *Inorg. Chim. Acta* **2008**, *361*, 3785.
(25) Yao, H.-C.; Gao, S.; Song, Y.; Zheng, L.-M.; Xin, X.-Q. *J. Solid State Chem.* **2004**, *177*, 4557.
(26) Cao, D. K.; Xie, X. J.; Li, Y. Z.; Zheng, L. M. *Dalt. Trans.* **2008**, *37*, 5008.
(27) Rabu, P.; Drillon, M. *Magnetic Organic—Inorganic Hybrid Materials. Synthesis, Structures, and Properties*; American Scientific Publishers: Stevenson Ranch, CA, 2003; Vol. 1.
(28) Rabu, P.; Drillon, M. *Layered Organic-Inorganic Materials. A Way Towards Controlling Magnetism*; Wiley: Weinheim, Germany, 2004.
(29) Di, W.; Ferreira, R. A. S.; Willinger, M.-G.; Ren, X.; Penna, N. *J. Phys. Chem. C* **2010**, *4*, 6290.
(30) Barber, P.; Houghton, H.; Balasubramanian, S.; Anguchamy, Y. K.; Ploehn, H. J.; zur Loye, H.-C. *Chem. Mater.* **2009**, *21*, 1303–1310.
(31) Poojary, D. M.; Zhang, B.; Cabeza, A.; Aranda, M. A. G.; Bruque, S.; Clearfield, A. *J. Mater. Chem.* **1996**, *6*, 639.
(32) Figueroa, C. A. S., P. J.; Morando, M. A.; Blesa, J. *J. Colloid Interface Sci.* **2000**, *225*, 403.
(33) Carlino, S.; Hudson, M. J.; Husain, S. W.; Knowles, J. A. *Solid State Ionics* **1996**, *84*, 117–129.
(34) Hix, G. B.; Harris, K. D. M. *J. Mater. Chem.* **1998**, *8*, 579–584.
(35) Cui, Z.; Zhang, F.; Wang, L.; Xu, S.; Guo, X. *Langmuir* **2010**, *26*, 179–182.
(36) Hatton, B. D.; Landskron, K.; Hunks, W. J.; Bennett, M. R.; Shukaris, D.; Perovic, D. D.; Ozin, G. A. *Mater Today* **2006**, *9*, 22.
(37) Maex, K.; Bakalanov, M. R.; Shamiryan, D.; Iacopi, F.; Brongersma, S. H.; Yanovitskaya, Z. S. *J. Appl. Phys.* **2003**, *93*, 8793.
(38) Treichel, H.; Goonetilleke, C. *Adv. Eng. Mater.* **2001**, *3*, 461.
(39) Shannon, R. D.; Fischer, R. X. *Phys. Rev. B* **2006**, *73*, 235111.

AM1003987